BNL-211489-2019-JAAM

Fe0.36(4)Pd0.64(4)Se2: Magnetic Spin-Glass Polymorph of FeSe2 and PdSe2 Stable at Ambient Pressure

C. Petrovic,

To be published in "INORGANIC CHEMISTRY"

March 2019

Condensed Matter Physics and Materials Science Department

Brookhaven National Laboratory

U.S. Department of Energy

USDOE Office of Science (SC), Basic Energy Sciences (BES) (SC-22)

DISCLAIMER

$Fe_{0.36(4)}Pd_{0.64(4)}Se_2$: Magnetic spin-glass polymorph of $FeSe_2$ and $PdSe_2$ stable at ambient pressure

Jianjun Tian,[1,2] Valentin N. Ivanovski,[3] David Szalda,[4] Hechang Lei,[5] Aifeng Wang,[1] Yu Liu,[1] Weifeng Zhang,[2] Vasil Koteski,[3] and Cedomir Petrovic[1]*

[1] *Condensed Matter Physics and Materials Science Department, Brookhaven National Laboratory, Upton, New York 11973, USA*

[2] *Henan Key Laboratory of Photovoltaic Materials and School of Physics & Electronics, Henan University, Kaifeng 475004, China*

[3] *Vinca Institute of Nuclear Sciences, University of Belgrade, Belgrade 11001, Serbia*

[4] *Department of Natural Sciences, Baruch College, CUNY, New York, New York 10010-5585, United States*

[5] *Department of Physics, Renmin University of China, Beijing 100872, China*

E-mail: petrovic@bnl.gov

Abstract

We report about the synthesis and characterization of $Fe_{0.36(4)}Pd_{0.64(4)}Se_2$ with a pyrite-type structure. $Fe_{0.36(4)}Pd_{0.64(4)}Se_2$ was synthesized using ambient pressure flux crystal growth methods even though Pa3 is high pressure polymorph for both $FeSe_2$ and $PdSe_2$. Combined experimental and theoretical analysis reveal magnetic spin glass state below 23 K in 1000 Oe that stems from random Fe/Pd occupancies on the same atomic site. The frozen-in magnetic randomness contributes significantly to electronic transport. Electronic structure calculations

*To whom correspondence should be addressed

confirm dominant *d*-electron character of hybridized bands and large density of states near the Fermi level. Flux-grown single crystal alloys in Pd-Fe-Se atomic system therefore open new pathway for exploring different polymorphs in crystal structures and their novel properties.

INTRODUCTION

Electronic systems where magnetic atoms are in between localized and itinerant are subject of competing tendencies of carrier hopping between atomic orbitals that promotes itinerancy and electronic repulsion that stimulates localization.[1–3] This is of particular interest in superconducting and thermoelectric Fe pnictides and chalcogenides that feature coexistence of localized and itinerant *d* orbitals.[4,5] Whereas external parameters such as chemical substitutions, pressure and magnetic field are common tuning parameters, different crystal structure polymorphs are seldom used to tip the balance of interactions due to difficulties in high-pressure materials synthesis and characterization.[6–9]

Here we use ambient-pressure synthesis methods to grow $Fe_{0.36(4)}Pd_{0.64(4)}Se_2$ single crystals with pyrite structure. Whereas $FeSe_2$ and $PdSe_2$ crystallize in Pnnm and Pbca space groups at ambient pressure, respectively, $FeSe_2$ and $PdSe_2$ polymorphs with pyrite space group Pa3 are synthesized only at high pressure.[10–13] $FeSe_2$ synthesized at high pressure is a semiconductor with zero effective moment $\mu_{eff} = 0$, whereas pyrite $PdSe_2$ is 13.1 K superconductor at 21.2 GPa.[12,14,15] In contrast to end members, magnetic properties of $Fe_{0.36(4)}Pd_{0.64(4)}Se_2$ single crystal alloy indicate weak spin-glass behavior with spin freezing temperature T_f below 30 K in 1000 Oe. Phonon-dominated metallic resistivity shows resistance upturn at low temperatures due to additional scattering caused by frozen-in magnetic randomness in the spin glass state, similar to glassy quasicrystals.[16] Our results suggest that ambient pressure synthesis conditions can be used to synthesize high-pressure polymorphs of transition metal chalcogenides with new emergent properties.

EXPERIMENT

Synthesis.

Single crystals of $Fe_{0.36(4)}Pd_{0.64(4)}Se_2$ were grown using flux method for intermetalics from excess selenium melts with Fe:Pd:Se = 1:1:10 mol ratio.[17] Variance of raw materials stoichiometry among 1:1:10, 1:2:10, 3:1:10 and 1:3:10 resulted also in the pyrite-type crystal structure where metal stoichiometry was identical to $Fe_{0.36(4)}Pd_{0.64(4)}Se_2$ within the resolution of structure and composition analaysis, suggesting relatively wide region of stability at the Fe-Pd-Se ternary alloy phase diagram where the only known Fe-Pd-Se compound is $FePd_2Se_2$ that crystallizes in Ibam space group.[18] The source elements were put into an alumina crucible, and then sealed in a quartz tube with a partial pressure of argon gas. The heating temperature for the tube was ramped to 800 °C and then cooled to 300 °C over 100 hours where crystals were decanted from liquid. Black single crystals up to 1.5 × 1.5 × 1.4 mm^3 can be grown.

Structure and Composition Analysis.

Chemical compositions of crystals was verified by the energy-dispersive x-ray spectroscopy (EDX) on JEOL LSM-6500 scanning electron microscope. Single crystal measurement using a Bruker Kappa Apex II diffractometer was performed on a crystal [0.50·0.50·0.30] mm^3 mounted at the end of a glass fiber. Data collected at 293 K indicated cubic symmetry and space group Pa3. The structure of $Fe_{0.36(4)}Pd_{0.64(4)}Se_2$ was solved by direct methods.[19] In the least-squares refinement, anisotropic temperature parameters were used for all atoms. Since the palladium and iron atoms occupy the same special position, the anisotropic thermal parameters for these two atoms were constrained to be equal. The data were corrected for absorption using the multi-scan method. Table 1 contains details of the single crystal data collection and refinement. Powder X-ray diffraction data of the sample were collected by a Rigaku Miniflex X-ray diffractometer with Cu K_α radiation (λ =0.15418 nm). The data were used to confirm bulk phase identity and purity of the samples with RIETICA software.[20]

Electrical, Thermal Transport, Magnetic and Mössbauer Measurements.

Electrical and thermal transport, heat capacity and magnetic measurements were carried out in Quantum Design PPMS-9 and MPMS-XL5. Sample mass and dimensions were measured by Mettler Toledo XP2U balance and by Nikon SMZ-800 optical microscope with 10 μm resolution. Consequently the relative errors arising from the contact size and position were about 2% in resistivity and about 1% in magnetic and heat capacity measurements. The relative error for both κ and S was less than 5% based on a Ni standard measured under identical conditions. For $Fe_{0.36(4)}Pd_{0.64(4)}Se_2$, the measurement of the Mössbauer effect in was performed in transmission geometry using a ^{57}Co(Rh) source calibrated by Fe foil at room temperature (RT). The spectrum of pulverized crystal was analyzed using WinNormos-Site software package.[21] The isomer shift value is in reference to metallic α-Fe δ =0.

Electronic Structure Calculations.

The electronic structure of $Pd_{0.64}Fe_{0.36}Se_2$ was calculated within the density functional theory (DFT), as implemented in the Vienna *ab initio* simulation package VASP.[22] In VASP, the core electrons are treated by using projector augmented-wave (PAW) pseudopotentials,[23] while the valence electrons are represented via a plane wave set. To model the $Pd_{0.64}Fe_{0.36}Se_2$ ternary system, we searched for lowest energy structures calculating several supercells in $3\times1\times1$, $3\times2\times1$, and $2\times2\times2$ geometry with different spatial distributions of Pd and Fe atoms.

We optimized the lattice parameters of the pyrite-type $FeSe_2$ and $FePd_2$ end-compounds in the first step of our calculations. The cut-off energy of the basis set was 350 eV, while a smaller cut-off of 250 eV was used for the supercells. The *k*-point mesh for sampling the Brillouin zone was set to $9\times9\times9$ for the pure systems, and was proportionally reduced for the supercells. The generalized gradient approximation (GGA) in the improved PBE implementation[24] was employed to describe the exchange and correlation energy. Before constructing the supercells, the lattice parameter of $Pd_{0.64}Fe_{0.36}Se_2$ (6.117 Å) was determined by a linear interpolation of the calculated $FeSe_2$ (5.823 Å) and $FePd_2$ (6.264 Å) parameters. All atoms in the supercells were allowed to relax with a force

criterion of 0.03 eVÅ^{-1}.

The hyperfine parameters and DOS calculations were carried out with the WIEN2K[25] code in the optimized $Pd_{0.64}Fe_{0.36}Se_2$ supercell. WIEN2K is an all-electron code based on the DFT and augmented plane wave (APW) plus local orbitals (lo), especially suitable for calculations of electric field gradients and magnetic hyperfine fields where accurate electronic structure determination is needed. The RK_{max} parameter that determines the size of the APW+lo basis set was 8. Muffin-tin spheres of 2.43, 2.26, and 2.15 a.u. were chosen for Pd, Fe, and Se, respectively. The forces between the atoms were converged to less than 0.04 eVÅ^{-1}. The hyperfine parameters were then calculated from the self-consistent all-electron charge density.[26] The isomer shift of iron was obtained by matching the electron density at the nucleus with the reference value of bcc iron.[27]

RESULTS AND DISCUSSION

Structure and Compostion.

The average atomic composition from EDX spectra confirmed homogeneous crystals with Fe:Pd:Se = 0.33(4):0.67(4):2.00. The refinement of the structure including the occupancy factors for the palladium and iron atoms resulted in a formula of $Fe_{0.40}(4)Pd_{0.60}(4)Se_2$ for the crystal, pyrite-type crystal structure with space group Pa3, and lattice constant a = 0.60542(3) nm. The formula Pd0.64(4)Fe0.36(4)Se2, consistent with error bars for both measurement is therefore used throughout the text. The lattice parameter is larger than those of $FeSe_2$ [a= 0.5785(9) nm] with Pa3 space group prepared at high pressure.[11] Powder XRD pattern at room temperature is shown in Fig. 1(a), confirming bulk phase purity, Pa3 space group and lattice parameter a =0.6048(3) nm, in agreement with single crystal X-ray diffraction.

Crystal structure of $Fe_{0.36(4)}Pd_{0.64(4)}Se_2$ likely features random occupancy of Pd and Fe atoms on the same atomic position site in the unit cell [Fig. 1(b)]. To verify this, Mössbauer spectroscopy was used to provide additional information of the Fe atomic environment in the lattice. Coordination polyhedra of a metal ion M in MSe_2 with Pa3 symmetry consists of 6 selenium ions. The

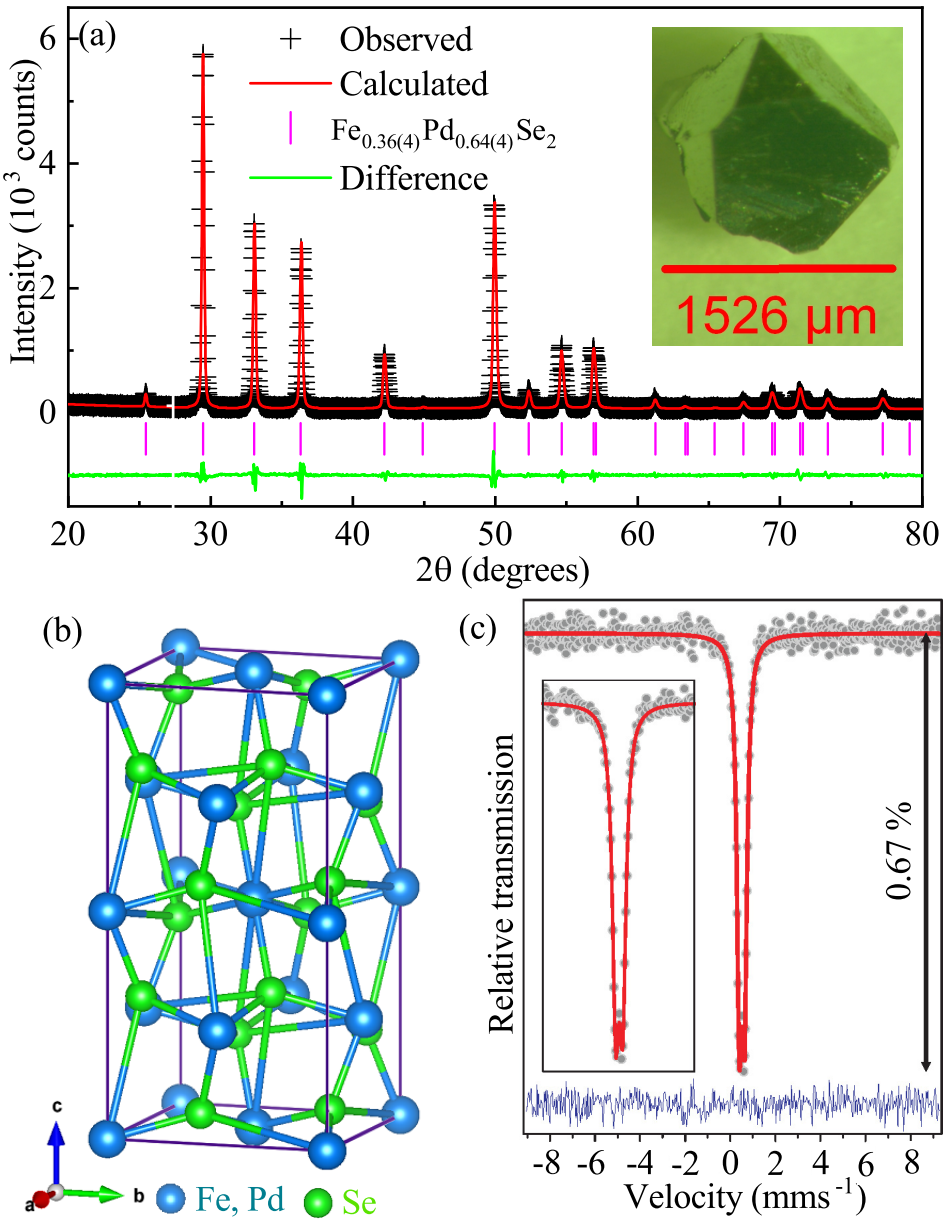

Figure 1: (a) Powder XRD patterns of $Fe_{0.36(4)}Pd_{0.64(4)}Se_2$ and fit to Pa3 model. The data are shown by (+), fitting and difference curves are given by the red and green solid line below, respectively. Inset shows photo of a typical single crystal. (b) Crystal structure of $Fe_{0.36(4)}Pd_{0.64(4)}Se_2$ in Pa3 space group. Metal atoms (Fe,Pd) are coordinated by six Se atoms, forming a distorted $(Fe,Pd)Se_6$ octahedron. Note that 2 cell units are shown along the c axis. (c) Mössbauer spectrum at 294 K of the $Fe_{0.36(4)}Pd_{0.64(4)}Se_2$ pyrite type structure. The observed data are presented by the gray solid circles, fit is given by the red solid line, and difference is shown by the blue solid line. The absolute value of difference is less than 0.036%. Vertical arrow denotes relative position of the lowest experimental point with respect to the background, i.e. the relative transmission. The inset shows the zoom of signal from -2 up to 3 mms^{-1}.

Table 1: Crystallographic Collection and Refinement Data for $Fe_{0.36(4)}Pd_{0.64(4)}Se_2$ Single Crystal.

Chemical Formula				$Fe_{0.36(4)}Pd_{0.64(4)}Se_2$
Formula Mass (g/mol)				244.10
Crystal System				Cubic
Space Group				Pa3 (No. 205)
a (Å)				6.0542(3)
Z				4
Density (g/cm^3)				7.306
Temperature (K)				293(2)
Wavelength (Å)				0.71073
Volume (Å^3)				221.907(19)
F(000)				424
Absorption coefficient (mm^{-1})				40.075
Crystal size (mm)				0.50 x 0.5 x 0.3
Theta range for data collection(°)				5.84 $\sim$ 32.55
Limiting indices				-9<=h<=9, -9<=k<=9, -9<=l<=9
Reflections collected / unique				5719 / 138 [R(int) = 0.0641]
Completeness to theta = 32.55				100.0%
Absorption correction				Semi-empirical from equivalents
Max. and min. transmission				0.7464 and 0.3373
Refinement method				Full-matrix least-squares on F^2
Data / restraints / parameters				138 / 0 / 9
Goodness-of-fit on F^2				1.249
Final R indices [I>2sigma(I)]				R1 = 0.0180, wR2 = 0.0471
R indices (all data)				R1 = 0.0184, wR2 = 0.0473
Extinction coefficient				0.041(4)
Largest diff. peak and hole (e.Å^{-3})				0.945 and -1.084
$R_1 = \Sigma\|\|F_o\|-\|F_c\|\|/\Sigma\|F_o\|$				$wR_2 = \Sigma[w(\|F_o\|^2-\|F_c\|^2)^2]/\Sigma[w\|F_o{}^2\|^2]$
Atom	site	x	y	z
Fe	4a	0.5	0.5	0
Pd	4a	0.5	0.5	0
Se	8c	0.38441(5)	0.11559(5)	0.88441(5)

regular octahedra is commonly tilted by about 5° from the ideal values and is surrounded by a metal shell of 12 cations.[28] Assuming random distribution of Fe among the Pd, the number of Fe in the nearest cation shell (n) is described by the binomial distribution:

$$P(n) = \binom{12}{n} c^n (1-c)^{12-n} \tag{1}$$

where is c = 1/3. The significant probabilities are obtained for n = 2, 3, 4, 5, and 6. The assumption of multimodal distribution of quadrupole splitting was tested on a 2×2×2 supercell with random substitution of eleven Pd ions with Fe ions. We then compared the magnitudes of the largest component of electric field gradient (*EFG*) tensor (V_{zz}) at Fe nuclei at 0 K. The selected combination gives V_{zz} values between -3.6 and -1.7 10^{21} Vm^{-2} depending on the number of Fe ions in the metal shell (NNFe = 1, 2, ... ,6) and on a permutation of their positions within metal shell. This multimodal distribution of quadrupole splitting (Δ) is not in agreement with the analysis of the Mössbauer spectrum, which shows that a model with one doublet is only suitable [Fig. 1(c)]. The measured hyperfine parameters are: δ = 0.520(2) mms^{-1} and (Δ) = 0.230(3) mms^{-1}. The width of the two Lorentz lines of the doublet is 0.267(5) mms^{-1}, with the line area ratio of 0.97(3). Unequal line areas occur due to the effect of sample preparation of a crushed monocrystal. Taking into account that the widest line of the calibrated α-Fe spectrum has a value of 0.243(3) mms^{-1}, the measured narrow doublet refers to a well ordered equivalent Fe positions in the $Fe_{0.36(4)}Pd_{0.64(4)}Se_2$ pyrite type structure. This implies an uniform distribution of Fe ions and at the same time excludes the magnetic impurity phases of iron.

This is indeed in agreement with our calculations, where the supercell with the lowest total energy corresponds to a uniform distribution of Fe atoms within the metal sublattice. Our calculation at T = 0 K gives chemical shift δ = 0.45 mms^{-1}, V_{zz} = -1.61 10^{21} Vm^{-2}, and asymmetry parameter η = 0.24 ($\eta = |(V_{yy} - V_{xx})/V_{zz}|$). For comparison we used the expression for the energy difference (i.e. Δ) between the ^{57}Fe ($|I = 3/2>$) sublevels:[29]

$$\Delta = \frac{1}{2} eQV_{zz}\sqrt{1+\frac{\eta^2}{3}} \tag{2}$$

According to equation 2 the recalculated value of $\Delta = 0.270$ mms^{-1} is obtained by using the ^{57}Fe nuclear quadrupole moment value of $Q = 0.16$ b and 1 mms^{-1} = 48.075 neV.[26,29] The calibration constant for ^{57}Fe, $\alpha = 0.291$ mms^{-1}a.u.[3] is used to recalculate values of chemical shift δ.[30] The V_{zz} calculated result is in good agreement with the experimental result when temperature contribution is taken into account. The second order Doppler shift correction (δ_{SOD}) reduces δ_{CS} at $T > 0$ K. Hence, the measured δ at room temperature ($\delta = \delta_{CS} + \delta_{SOD}$) could indicate that the Fe 4s orbitals is more depopulated than the Fe 3d orbitals with temperature increase.[31]

It could be useful to compare the Mössbauer spectroscopy result of $Fe_{0.36(4)}Pd_{0.64(4)}Se_2$ to the end-member $FeSe_2$ with pyrite structure. Given that there are no experimental data for pyrite $FeSe_2$ at ambient pressure, we calculated its hyperfine parameters: chemical shift δ = 0.477 mms^{-1}, V_{zz} = -4.1 10^{21} Vm^{-2}, and η = 0. Using equation 2 we obtain Δ = 0.682 mms^{-1}, which is about three times larger when compared to $Fe_{0.36(4)}Pd_{0.64(4)}Se_2$. In comparison with the results of hyperfine parameters measured at room temperature on FeX_2 (X = S, Se) in both pyrite and marcasite structure, the calculated Δ of pyrite $FeSe_2$ is in agreement with the one of pyrite FeS_2, while chemical shift δ corresponds to marcasite $FeSe_2$.[32] Even though the Fe site symmetry is lower in marcasite $\left(C_{2h}, \frac{2}{m}\right)$ when compared to pyrite polymorph $\left(C_{3i}, \bar{3}\right)$, the values of δ and Δ are somewhat higher for both pyrite compounds. A more populated $4s$ state of Fe in marcasite FeS than in pyrite structure causes larger δ at the latter polymorph.[33] This might point to the enhanced hybridization of the chalcogen sp valence states with Fe $3d - e_g$ states.[34] While there is covalence in the iron-chalcogen bond, there is no indication of direct interaction between Fe-Fe ions which would produce disparity of population among the valence orbitals, i.e. a larger Δ.[33] Complete understanding of our result $\delta = 0.520(2)$ mms^{-1} and $\Delta = 0.230(3)$ mms^{-1}) requires further insight into local crystal structure. Our calculations indicate that the coordination polyhedron around Fe, as well as around Pd, is not distorted. The Fe-Se distances are distributed over a range of values, from 0.2366 nm to 0.2513 nm; note that the calculated Fe-Se distance in pure $FeSe_2$ is 0.2414 nm. All Fe-Se distances in $Fe_{0.36(4)}Pd_{0.64(4)}Se_2$ are shortened relative to the regular $PdSe_6$ octahedron.

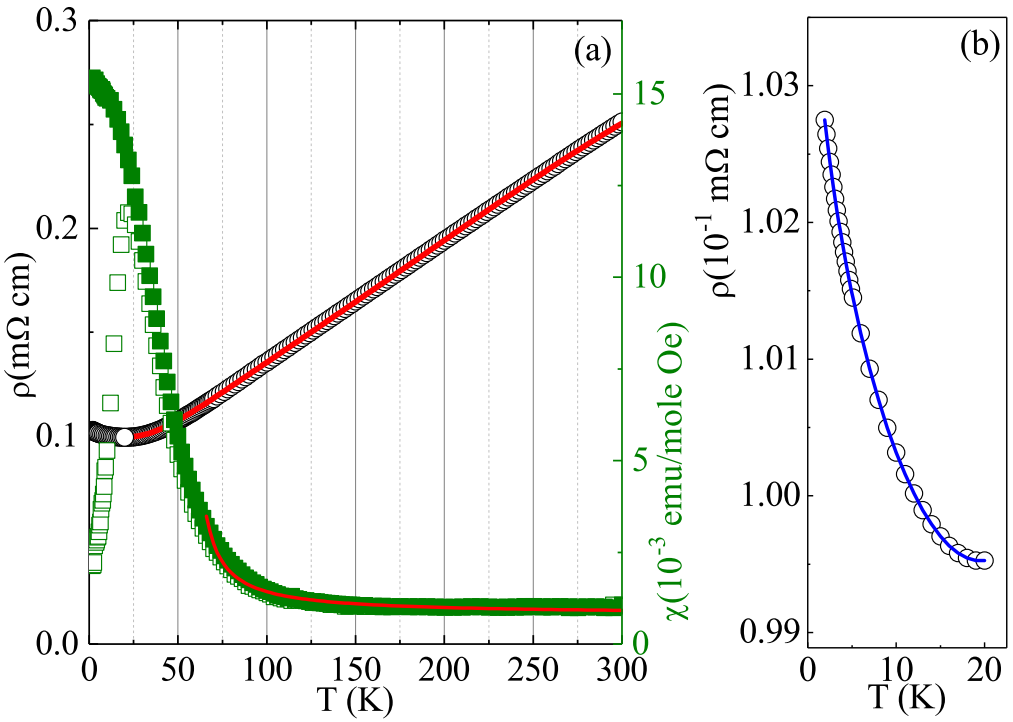

Figure 2: (a) Temperature dependence of resistivity $\rho(T)$ in zero-field and magnetic susceptibility $\chi(T)$ in 1000 Oe of $Fe_{0.36(4)}Pd_{0.64(4)}Se_2$. Zero-field-cooled and field-cooled data are shown by open and full symbols, respectively. Red line shows high temperature Bloch-Grüneisen and Curie-Weiss fits for $\rho(T)$ and $\chi(T)$, respectively. (b) Low-temperature $\rho(T)$ (open symbols) and fit (blue line, see text).

Electrical and Magnetic Properties.

Figure 2(a) shows the temperature dependence of the resistivity $\rho(T)$ of $Fe_{0.36(4)}Pd_{0.64(4)}Se_2$. The sample exhibits metallic resistivity from room temperature down to about 20 K. Further decrease in temperature results in weak increase in resistivity. The $\rho(T)$ curve above 25 K can be explained within the framework of Bloch-Grüneisen (BG) model of electron-phonon scattering:[35]

$$\rho(T) = \rho_0 + C_1(\frac{T}{\Theta_D})^5 \int_0^{\Theta_D/T} \frac{x^5}{(e^x-1)(1-e^{-x})}dx \quad (3)$$

where ρ_0 is the residual resistivity from defects and impurities when $T \to 0$, and the second term (BG) reflects the contributions from the electron−phonon interaction. C_1 is a constant reflecting the electron-phonon coupling strength and Θ_D is the Debye temperature of phonons that take part in the scattering process at high temperature. Good fit [red curve in Fig. 2(a)] indicates that the dominant scattering mechanism in $Fe_{0.36(4)}Pd_{0.64(4)}Se_2$ single crystal is electron-phonon intraband scattering.[35,36] Fitting parameters ρ_0 and C_1 are 0.0999(2) mΩ cm, 0.5751(1) mΩ cm respectively, and Θ_D is about 273.7(2) K. The magnetic susceptibility $\chi(T)$ of $Fe_{0.36(4)}Pd_{0.64(4)}Se_2$ single crystal in magnetic field shows irreversible behavior below 23 K in 1000 Oe indicating glassy transition [Fig. 2(a)], possibly induced by random occupancy of Fe/Pd atomic sites. The $\chi(T)$ above 60 K can be explained by the Curie-Weiss law: $\chi(T) = C/(T-\theta)+\chi_0$, where C is the Curie constant, θ is the Curie-Weiss temperature, and temperature independent χ_0 includes core diamagnetism, Pauli paramagnetism and Landau diamagnetism. The acquired values for C, θ and χ_0 are 0.027(1) emu mol^{-1} Oe^{-1} K, -55.75(1) K, and $8.06(1)\times10^{-4}$ emu mol^{-1} Oe^{-1}, respectively. A negative Curie-Weiss temperature indicates dominant antiferromagnetic interactions of the Weiss molecular field. The effective high-temperature moment acquired from the relationship $\mu_{eff} = 2.83\ (C/n)^{0.5}\mu_B$ (where n = 0.33 is the number of magnetic atoms in a molecular formula $Fe_{0.36(4)}Pd_{0.64(4)}Se_2$) is 0.81(1) μ_B/Fe. The $\chi(T)$ irreversible behavior is coincident with the low-temperature upturn in $\rho(T)$. This suggests close correlation of changes in bulk magnetic and transport properties.

Magnetic contribution to the resistivity in spin glass state can be detected in BT^2-$C_2T^{5/2}$ temperature dependence, where coefficients B and C_2 represent the strength of diffusive spin excitation.[37] Therefore, electron-electron scattering, and electron-phonon scattering contribute to the low-temperature resistivity:

$$\rho'(T) = \rho'_0 - m'_p\sqrt{T} + (BT^2 - C_2T^{5/2}) + BG \tag{4}$$

where the ρ'_0 is the residual resistivity, the second term arises from the Coulomb-enhanced electron-electron interaction in disordered systems,[38] the third term denotes the magnetic spin glass contribution, and the BG term depicts the scattering of conduction electron by phonons. The $\rho(T)$ curve below 20 K can be well fitted by using eq. (4) [Fig. 2(b)]. This is similar to NiMnSn and CuMn magnetic glass alloys.[39,40] The fitting parameters ρ'_0, m'_p, B, C_2, C' and Θ'_D are 0.1049(1) mΩ cm, 1.5572(8) $\mu\Omega$ cm $K^{-1/2}$, 3.3992(2) nΩ cm K^{-2}, 0.1234(3) nΩ cm $K^{-5/2}$, 0.2580(6) mΩ cm and 269.3(4) K respectively. When compared to NiMnSn and CuMn alloys, the $\sim\sqrt{T}$ is about one order of magnitude higher, implying stronger electron-electron interaction effects in $Fe_{0.36(4)}Pd_{0.64(4)}Se_2$.[39,40]

There is a linear field dependence of the magnetic susceptibility with no hysteresis at 300 K, an S-shaped loop and weak ferromagnetism in the M-H curve at 1.8 K, typical characteristics of magnetic spin glass [Fig. 3(a)].[41] However, an S-shaped loop also reveals a weak ferromagnetic component. Weak magnetic states are common in narrow-band materials.[42–45] The overall shape of the density of states (DOS) of $Fe_{0.36(4)}Pd_{0.64(4)}Se_2$ [Fig. 3(b)] is in agreement with possible weak magnetic polarization of itinerant states. It resembles the pure pyrite-type $PdSe_2$ DOS, especially around the Fermi level, but with considerable overall enhancement.[15] This is in contrast to pyrite-type $FeSe_2$.[14] As expected, Fe states dominate the partial density of states at the Fermi level whereas Pd contribution is about half when compared to Fe.

The S-shaped M-H curve at 1.8 K, the linear M-H behavior at 300 K and the antiferromagnetic Weiss temperatures illustrate the complex magnetism in $Fe_{0.36(4)}Pd_{0.64(4)}Se_2$. When localized electronic states give rise to magnetic moments in metals, Ruderman-Kittel-Kasuya-Yosida

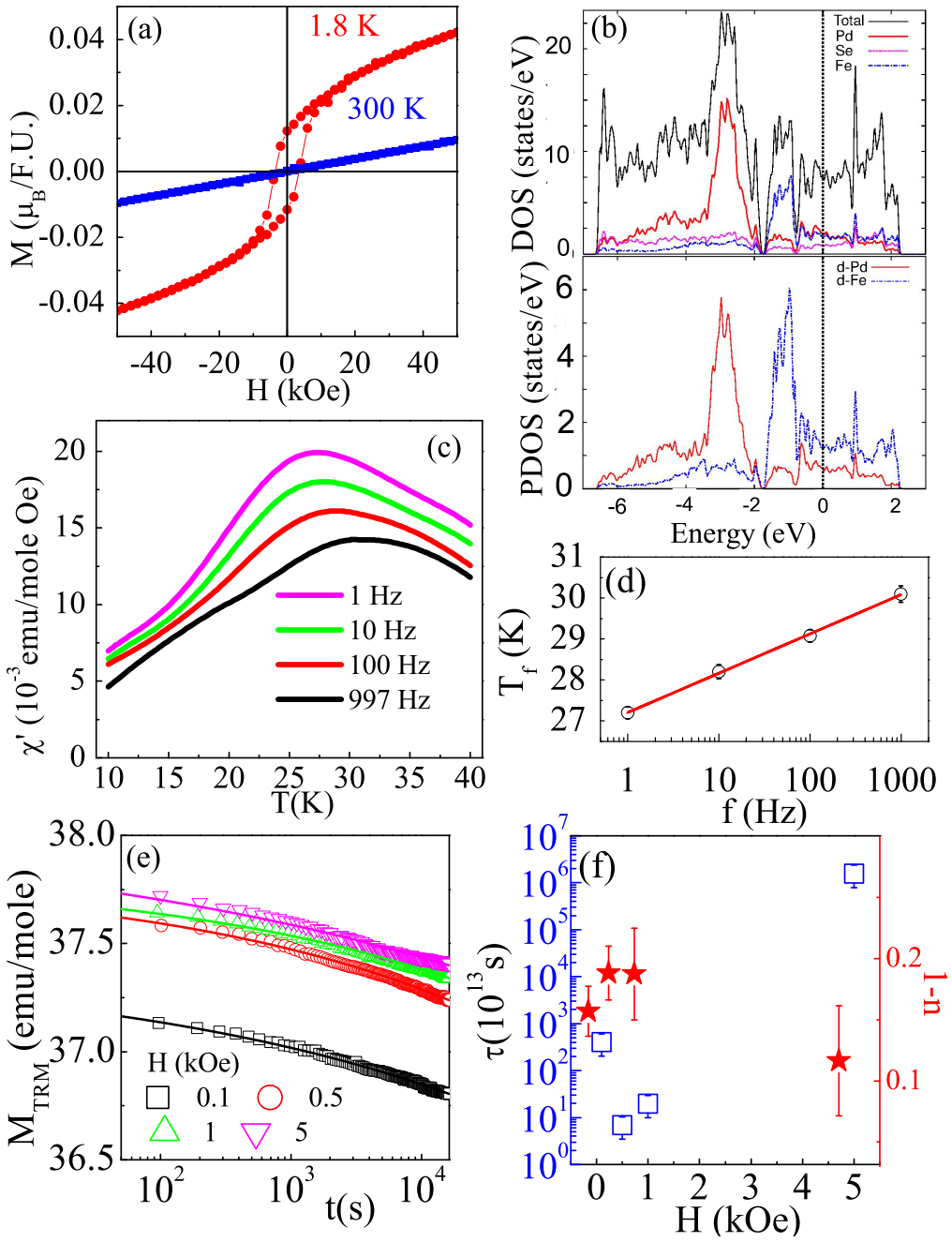

Figure 3: (a) Magnetization M-H curves at 1.8 K and 300 K of $Fe_{0.36(4)}Pd_{0.64(4)}Se_2$. (b) (top) Calculated density of states (DOS) for pyrite $Fe_{0.36(4)}Pd_{0.64(4)}Se_2$ using GGA. (bottom) Projected density of states (PDOS) for Fe and Pd d-states in $Fe_{0.36(4)}Pd_{0.64(4)}Se_2$. The vertical dashed line denotes the Fermi level. (c) Temperature dependence of ac susceptibility $\chi'(T)$ measured at four different frequencies in 1 Oe ac field. (d) Frequency dependence of T_f. The solid line is the linear fit to the T_f data. (e) Thermoremanent magnetization (TRM) as a function of time at 10 K t_w = 100 measured at dc field with fittings using stretched exponential function (solid lines). (f) H-field dependence of $\tau(s)$ (open squares) and $1-n$ (solid squares).

(RKKY) interaction mechanism could result in ferromagnetic (FM) or antiferromagnetic (AFM) order, depending on the magnetic moment distance and carrier density.[41,46] It is likely that there is a competition between ferromagnetic and antiferromagnetic interactions among localized states in $Fe_{0.36(4)}Pd_{0.64(4)}Se_2$ due to random and different Fe-Fe distances and carrier concentration changes in the investigated temperature range.

In a magnetic spin glass, spin interactions result in a highly irreversible and metastable state which is sensitive to time-dependent/ac magnetization. The peak in the real part of the ac susceptibility $\chi'(T)$ shows strong frequency dependence in an ac magnetic field [Fig. 3(c)]. As the frequency increases, the peak positions shift toward higher temperatures whereas the magnitude of $\chi'(T)$ decreases. This is a typical spin glass behavior.[41] From K=ΔT_f / $T_f \Delta log f$, from the frequency dependence of the peak shift fits we obtain K = 0.035(1) [Fig. 3(d)]. This value is consistent with the values between 0.0045 and 0.08 expected for a conventional spin glass system.[41] Figure 3(e) presents the magnetic field dependence of the thermoremanent magnetization (TRM). The sample was cooled from T = 40 K (above T_f) to 10 K (below T_f) in different magnetic fields, and then held for t_w = 100 s. Then, the magnetic field was removed and the magnetization decay $M_{TRM}(t)$ was measured. It is found that $M_{TRM}(t)$ decays slowly at 10 K; its value is nonzero even after several hours as expected for a spin glass.[41] The decay can be fitted with the formula: $M_{TRM}(t)$= M_0exp[-$(t/\tau)^{1-n}$], where M_0, τ and 1-n are the glassy component, the relaxation time and the critical exponent respectively. The acquired τ decreases up to 1 kOe and increases abruptly at 5 kOe, while $1-n$ value decreases with increasing H [Fig. 3(f)]. The attained $1-n$ value is in accordance with theoretical and experimental values found in other spin glass materials.[47]

Similar frequency dependence of ac susceptibility $\chi'(T)$ is also sometimes observed in superparamagnetic materials,[48] however the relation between T_f and f for the $Fe_{0.36(4)}Pd_{0.64(4)}Se_2$ follows the Vogel-Fulcher expression $(2\pi f)^{-1} = \tau_0 \exp(A/(T_f\text{-}T_g)$.[49–51] Here τ_0 is the microscopic flipping time of fluctuating spins, A is the energy-related parameter, and T_g is the spin-glass transition temperature. Good data fit [Fig. 4(a) inset] supports the spin glass state in $Fe_{0.36(4)}Pd_{0.64(4)}Se_2$ single crystals. The fitting parameters τ_0 and T_g are 1.63×10^{-8} s and 22.54 K. In addition, for

spin-glass systems, $T_f \sim f$ curve agrees with a critical power law $(2\pi f)^{-1} = \tau_0(T_f/\mathrm{T}_g\text{-}1)^{-z\upsilon}$,[41] where z is the dynamical exponent and υ is the correlation length critical exponent. A good fit is presented in Fig. 4(a) with parameters $\tau_0 = 3.89\times10^{-9}$, $T_g = 23.8$ K and $z\upsilon = 9.0$.

The $z\upsilon$ value is within the $5 \sim 10$ range expected for canonical spin glasses.[41] The τ_0 values obtained by the Vogel-Fulcher model and the critical power law are somewhat different from the 10^{-10} - 10^{-13} s in typical spin-glass systems,[52,53] whereas they are similar to those observed in frustrated $ZnFe_2O_4$ ($\tau_0 = 10^{-8}$).[51] The larger τ_0 likely arises from the frustration since, when compared to conventional spin-glass systems, geometrical frustration strengthens the spin correlations and enhances τ_0.[54]

Thermodynamic and Thermal Transport Properties.

Figure 4(b) displays the temperature dependence of specific heat for $Fe_{0.36(4)}Pd_{0.64(4)}Se_2$ single crystal. The absence of anomaly in thermal properties rules out the dominance of Kondo effect in scattering mechanism in magnetic glassy state. At high temperature, the heat capacity approaches the Dulong-Petit value of $3NR$ (where $N = 3$ is the atomic number in the chemical formula and R is the universal gas constant 8.314 J mol^{-1} K^{-1}). From the fit using the formula $C_p/T = \gamma + \beta T^2$ at low temperature [inset in Fig. 4(b)], the linear coefficient of specific heat γ is 8.34(6) mJ mol^{-1} K^{-2}. From $\beta = 0.13(5)$ mJ mol^{-1} K^{-4}, the Debye temperature is $\Theta_{DC} = (12\pi^4\mathrm{NR}/5\beta)^{1/3} =$ 306.4(2) K. However, considering large atom mass difference between Fe and Pd atoms, it is also instructive to consider specific heat in the whole temperature range using double-Debye model:

$$\begin{aligned} C_P(T) =& \gamma' T + 9R(N-s)\left(\frac{T}{\Theta_{D1}}\right)^3 \int_0^{\Theta_{D1}/T} \frac{x^4 e^x}{(e^x-1)^2} dx \\ &+ 9Rs\left(\frac{T}{\Theta_{D2}}\right)^3 \int_0^{\Theta_{D2}/T} \frac{x^4 e^x}{(e^x-1)^2} dx + MT^2 \end{aligned} \tag{5}$$

where Θ_{D1} and Θ_{D2} are the Debye temperature for each sublattice,[55,56] s is the number of oscillators in one sublattice (set to a fitting parameter), and the last MT^2 term denotes the contribution from the spin glass.[57] The $C_P(T)$ curve can be fitted well by using this model [Fig. 4(b),

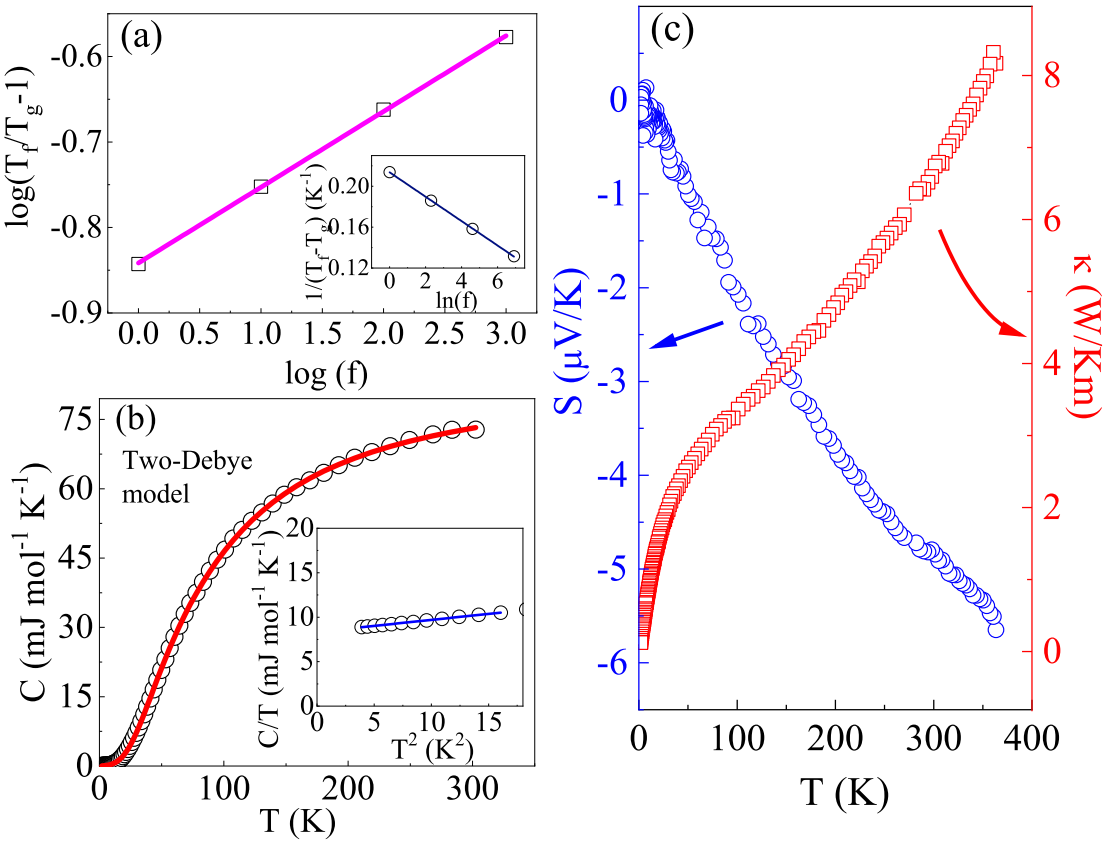

Figure 4: (a) Plot of $\log(T_f/T_g\text{-}1)$ vs. log(f) with the best fitting based on the critical-power law for $Fe_{0.36(4)}Pd_{0.64(4)}Se_2$, the inset shows $1/(T_f\text{-}T_g)$ vs. ln(f) and the best fitting with Vogel-Fulcher expresion. Temperature dependence of the heat capacity (b) and thermopower (S, left axis) and thermal conductivity (κ, right axis) (c) of $Fe_{0.36(4)}Pd_{0.64(4)}Se_2$ single crystals. Insets show low-temperature region.

red line]. The obtained s, γ', Θ_{D1} and Θ_{D2} are 0.98(1), 6.03(1) mJ mol^{-1} K^{-2}, 242.1(1) K, and 560.3(1) K, respectively, whereas M = 0.023(1) mJ mol^{-1} K^{-3}. This points to weak electronic mass enhancement and strong magnetic excitation component of linear specific heat. Moreover Debye temperature is in accordance with resistivity measurement [Fig. 1(a)] indicating that most phonons take part in the scattering process at high temperature.

Thermopower S and thermal conductivity κ of $Fe_{0.36(4)}Pd_{0.64(4)}Se_2$ are smaller than in marcasite $FeSe_2$ or pyrite $RuSe_2$ [Fig. 4(c)].[58,59] The sign of $S(T)$ indicates that the electron-like parts of the Fermi surface are dominant in electronic transport. The smaller values of thermal conductivity could be explained due to the alloy disorder that contributes to scattering of heat-carrying phonons.

Electronic Structure.

In $Fe_{0.36(4)}Pd_{0.64(4)}Se_2$ itinerant electrons have substantial d-character in hybridized bands with enhanced DOS near the Fermi level that could promote weak Stoner enhancement [Fig. 3(b)]. At the same time, Fe/Pd atoms are randomly distributed on metal sites, contributing to emergence of spin glass. It should be noted that the alloying in between $FeSe_2$ and $PdSe_2$ creates not only simple random distribution of atoms but also significant change in bond energies and ethalpies of formation so that high-pressure polymorph is stabilized. The alloying decreases the two long M-Se (M=Fe, Pd) distances of ambient pressure orthorhombic Pbca $PdSe_2$ and Pnnm $FeSe_2$ around each M atom to form six equivalent M-Se bonds of Pa3 $Fe_{0.36(4)}Pd_{0.64(4)}Se_2$.[10,11] This is in agreement with chemical pressure effect. In $PdSe_2$ pyrite structure is favored for unit cell volumes below 0.250 nm^3.[10] Moreover, pyrite-type crystal structure features face-centered cubic (fcc) AB_2 lattice where magnetic interactions are frustrated when the next-nearest-neighbor interactions are significant.[60–63] Both randomness and frustration contribute to the formation of the spin glass phase and therefore magnetic frustration could also be important for stabilization of spin glass in $Fe_{0.36(4)}Pd_{0.64(4)}Se_2$, as discussed above in the magnetic properties section.[64]

CONCLUSION

To summarize, we have synthesized single crystals of $Fe_{0.36(4)}Pd_{0.64(4)}Se_2$ with pyrite structure with random distribution of Fe/Pd atoms on metal sites. Weak magnetic spin glass is established at low temperatures whereas magnetic scattering stemming from frozen-in magnetic moment randomness is dominant in the glassy state. Pyrite structure for $FeSe_2$ and $PdSe_2$ commonly forms only at high pressures, suggesting that chemical pressure effects in $Fe_{0.36(4)}Pd_{0.64(4)}Se_2$ are important in stabilizing high-pressure polymorph.

ASSOCIATED CONTENT

Accesion codes CCDC 1878916 contains the supplementary crystallographic data for this paper.

AUTHOR INFORMATION

Corresponding Author Email:petrovic@bnl.gov **ORCID** Cedomir Petrovic: 0000-0001-6063-1881 **Author Contributions** The manuscript was written through contribution of all authors. All authors have given approval to the final version of the manuscript.

ACKNOWLEDGEMENTS

Research supported by the U.S. Department of Energy, Office of Basic Energy Sciences as part of the Computation Material Science Program through the Center for Computational Material Spectroscopy and Design and the Division of Materials Sciences and Engineering under Contract No. DE-SC0012704 (D. S). The Mössbauer work has been supported by the grant No. 171001 from the Ministry of Education, Science and Technological Development of the Republic of Serbia. One of the authors (Jianjun Tian) acknowledges the support from a scholarship of Faculty Training Abroad Program of Henan University.

References

(1) Kotliar, G.; Savrasov, S. J.; Haule, K.; Oudovenko, V. S.; Parcollet O.; Marianetti, C. A. Electronic Structure Calculations with Dynamical Mean-Field Theory. *Rev. Mod. Phys.* **2006**, *78*, 865-951.

(2) Shim, J. H.; Haule K.; Kotliar, G. Modeling the Localized-to-Itinerant Electronic Transition in the Heavy Fermion System $CeIrIn_5$. *Science* **2007**, *318*, 1615-1617.

(3) Biermann, S.; de Medici, L.; Georges, A. Non Fermi-Liquid Behavior and Double-Exhange Physics in Orbital-Selective Mott Systems. *Phys. Rev. Lett.* **2005**, *95*, 206401.

(4) Yin, Z. P.; Haule K.; Kotliar, G. Kinetic frustration and the nature of the magnetic and paramagnetic states in iron pnictides and iron chalcogenides. *Nat. Mater.* **2011**, *10*, 932-935.

(5) Tomczak, J. M.; Haule K.; Kotliar, G. Signatures of electronic correlations in iron silicide. *Proc. Natl. Acad. Sci. US* **2012**, *109*, 3243-3246.

(6) Montanari, E.; Righi, L.; Calestani, G.; Migliori, A.; Gilioli E.; Bolzoni, F. Room Temperature Polymorphism in Metastable $BiMnO_3$ Prepared by High-Pressure Synthesis. *Chem. Mater.* **2005**, *17*, 1765-1773.

(7) Machala, L.; Tucek J.; Zboril, R. Polymorphous Transformations of Nanometric Iron(III) Oxide: A Review. *Chem. Mater.* **2011**, *23*, 3255-3272.

(8) Sheng,H. W.; Liu, H. Z.; Cheng, Y. Q.; Wen, J.; Lee, P. L.; Luo, W. K.; Shastri, D.; Ma, E. Polymorphism in a metallic glass. *Nat. Mater.* **2007**, *6*, 192-197.

(9) Margadonna, S.; Takabayashi, Y.; Ohishi, Y.; Mizuguchi, Y.; Takano, Y.; Kagayama, T.; Nakagawa, T.; Takata M.; Prassides, K. Pressure evolution of the low-temperature crystal structure and bonding of the superconductor FeSe (T_c = 37 K). *Phys. Rev. B* **2009**, *80*, 064506.

(10) Soulard, C.; Rocquefelte, X.; Petit, P. E.; Evain, M.; Jobic, S.; Itie, J. P.; Munsch, P.; Koo, H. J.; Whangbo, M. H. Experimental and Theoretical Investigation on the Relative Stability of the PdS_2 and Pyrite-Type Structures of $PdSe_2$. *Inorg. Chem.* **2004**, *43*, 1943-1949.

(11) Bither, T. A.; Bouchard, R. J.; Cloud, W. H.; Donohue, P. C.; Siemons, W. J.; Transition metal pyrite dichalcogenides. High-pressure synthesis and correlation of properties. *Inorg. Chem.* **1968**, *7*, 2208-2220.

(12) Larchev, V. N.; Popova, S. V. Polymorphism of palladium dichalcogenides at high pressures and temperatures. *Inorg. Mater.* **1978**, *14*, 611-612.

(13) Bither, T. A.; Prewitt, C. T.; Gilson, J. L.; Bierstedt, P. E.; Flipen, R. B.; Young, H. S. New transition metal dichalcogenides formed at high pressure. *Solid State Comm.* **1966**, *4*, 533-535.

(14) Gudelli, V. K.; Kanchana, V.; Vaitheeswaran, G.; Valsakumar M. C.; Mahanti, S. D. Thermoelectric properties of marcasite and pyrite FeX_2 (X = Se, Te): a first principle study. *RSC Adv.* **2014**, *4*, 9424-9431.

(15) ElGhazali, M.; Naumov, P. G.; Mirhosseini, H.; Suss, V.; Muchler, L.; Schnelle, W.; Felser, C.; Medvedev, S. A. Pressure-induced superconductivity up to 13.1 K in the pyrite phase of palladium diselenide $PdSe_2$. *Phys. Rev. B* **2017**, *96*, 060509.

(16) Fisher, I. R.; Cheon, K. O.; Panchula, A. F.; Canfield, P. C.; Chernikov, M.; Ott H. R.; Dennis, K. Magnetic and transport properties of single-grain R-Mg-Zn icosahedral quasicrystals [R = Y, $(Y_{1-x}Gd_x)$, $(Y_{1-x}Tb_x)$, Tb, Dy, Ho, and Er]. *Phys. Rev. B* **1999**, *59*, 308-321.

(17) Fisk Z; Remeika J. P. Growth of single crystals from molten metal fluxes. *Handbook on the Physics and Chemistry of Rare Earths* **1989**, *12*, 53-70.

(18) Pocha, R.; Löhnhert, C.; Johrendt, D.; Fisher, The metal-rich palladium chalcogenides

Pd_2MCh_2 (M = Fe, Co, Ni; Ch = Se, Te): Crystal structure and topology of the electron density. *J. Solid State Chem.* **2007**, *180*, 191-197.

(19) Sheldrick, G. M. Siemens Analytical Instruments, Inc.: Madison, WI, 1994.

(20) Hunter, G. RIETICA, A Visual Rietveld Program. *International Union of Crystallography Commission on Powder Diffraction Newsletter* **1998**, *20*, 16.

(21) Brand, R. Winnormos Mössbauer Fitting Program; Universität Duisburg: Duisburg, Germany, 2008.

(22) Kresse, G. G.; Furthmller, J. Efficient iterative schemes for ab initio total-energy calculations using a plane-wave basis set. *Phys. Rev. B* **1996**, *54*, 11169-11186.

(23) Blochl, P. E. Projector augmented-wave method. *Phys. Rev. B* **1994**, *50*, 17953-17979.

(24) Perdew, J. P.; Burke K.; Ernzehof, M. Generalized Gradient Approximation Made Simple. *Phys. Rev. Lett.* **1996**, *77*, 3865-3868.

(25) Blaha, P.; Schwarz, K.; Madsen, G.; Kvasnicka, O.; Luitz, J. Wien2k, An Augmented Plane Wave Local Orbitals Program for Calculating Crystal Properties; Techn. Universität Wien, Austria, 2001.

(26) Dufek, P.; Blaha P.; Schwarz, K. Determination of the Nuclear Quadrupole Moment of ^{57}Fe. *Phys. Rev. Lett.* **1995**, *75*, 3545-3548.

(27) Blaha, P. Calculations of Mössbauer parameters in solids by DFT bandstructure calculations. *Journal of Physics: Conference Series* **2010**, *217*, 012009.

(28) Podberezskaya, N. V.; Magarill, S. A.; Pervukhina, N. V.; Borisov, S. V. Crystal Chemistry of Dichalcogenides MX_2. *J. Struct. Chem.* **2001**, *42*, 654.

(29) Chen, Y. L.; Yang, D. P. Mössbauer Effect in Lattice Dynamics: Experimental Techniques and Applications; John Wiley & Sons: Germany, 2007.

(30) Wdowik,U. D.; Ruebenbauer, K. Calibration of the isomer shift for the 14,4 keVtransition in ^{57}Fe using the full-potential linearized augmented plane-wave method. *Phys. Rev. B* **2007**, *76*, 155118.

(31) Menil F. Systematic trends of the ^{57}Fe Mössbauer isomer shifts in (FeO_n) and (FeF_n) polyhedra. Evidence of a new correlation between the isomer shift and the inductive effect of the competing bond T-X ($\longrightarrow$ Fe) (where X is O or F and T any element with a formal positive charge). *J. Phys. Chem. Solids* **1985**, *46*, 763-789.

(32) Temperley, A.; Lefevre, H. The Mössbauer effect in marcasite structure iron compounds. *J. Phys. Chem. Solids.* **1966**, *27*, 85-92.

(33) Schmokel, M. S.; Bjerg, L.; Cenedese, S.; Jorgensen, M. R. V., Chen, Y. S., Overgaard, J.; Iversen, B. B.; Atomic properties and chemical bonding in the pyrite and marcasite polymorphs of FeS_2: a combined experimental and theoretical electron density study. *Chem. Sci.* **2014**, *5*, 1408-1421.

(34) Eyert, V.; Höck, K. H.; Fiechter, S.; Tributsch, H. Electronic structure of FeS_2: The crucial role of electron-lattice interaction. *Phys. Rev. B* **1998**, *57*,6350-6359.

(35) Blatt, F. J. Physics of Electronic Conduction in Solids; McGraw-Hill: New York, 1968.

(36) Goetsch, R. J.; Anand, V. K.; Pandey A.; Johnston, D. C. Structural, thermal, magnetic, and electronic transport properties of the $LaNi_2(Ge1-xP_x)_2$ system. *Phys. Rev. B* **2012**, *85*, 054517.

(37) Fischer, K. H. On the electrical resistivity of spin glasses. *Z. Phys. B* **1979**, *34*, 45-53.

(38) Lee, P. A.; Ramakrishnan, T. V. Disordered electronic systems. *Rev. Mod. Phys.* **1985**, *57*, 287-337.

(39) Singh, S.; Pal, S.; Biswas, C. Disorder iduced resistivity anomaly in $NiMn_{1+x}Sn_{1-x}$. *J. Alloys and Compd.* **2014**, *616*, 110-115.

(40) Chakraborty S.; Majumdar, A. K. Resistivity minima in concentrated γ-$Cu_{100-x}Mn_x$ alloys ($36 \leq x \leq 83$). *Phys. Rev. B* **1996**, *53*, 6235-6239.

(41) Mydosh, J. A. Spin Glasses: An Experimental Introduction; Taylor & Francis: London, 1993.

(42) De Long, L. E.; Huber J. G.; Bedell, K. S.; Criteria for the occurence of ferromagnetism and weak magnetic order in narrow-band metals. *J. Magn. Magn. Mater* **1991**, 99, 171-189.

(43) Muro, Y.; Haizaki, Y.; Kim, M. S.; Umeo, K.; Tou, H.; Sera, M.; Takabatake, T. Heavy-fermion weak-ferromagnet YbRhSb. *Phys Rev. B* **2004**, *69*, 020401.

(44) Aplesnin, S. S.; Ryabinkina, L. I.; Abramova, G. M.; Romanova, O. B.; Vorotynov, A. M.; Velikanov, D. A.; Kiselev, N. I.; Balaev, A. D.; Conductivity, weak ferromagnetism, and charge instability in an α-MnS single crystal. *Phys. Rev B* **2005**, *71*, 125204.

(45) Mitsuda, A.; Goto, T.; Yoshimura, K.; Zhang, W.; Sato, N.; Kosuge K.; Wada, H. Weak ferromagnetism induced by pressure in $Yb_{0.8}Y_{0.2}InCu_4$. *J. Phys. Chem. Solids* **2002**, *63*, 1211-1213.

(46) Eggenkamp, P. J. T.; Swagten, H. J. M.; Story, T.; Litvinov, V. I.; Swĺźste, C. H. W.; de Jonge, W. J. M. Calculations of the ferromagnet-to-spin-glass transition in diluted magnetic systems with an RKKY interaction. *Phys. Rev. B* **1995**, *51*, 15250-15259.

(47) Chu, D.; Kenning, G. G.; Orbach, R. Dynamic measurements in a Heisenberg spin glass: CuMn. *Phys. Rev. Lett.* **1994**, *72*, 3270-3273.

(48) Subhankar, B.; Wolfgang, K. Supermagnetism. *J. Phys. D: Appl. Phys.* **2009**, *42*, 013001.

(49) Souletie, J.; Tholence, J. L. Critical slowing down in spin glasses and other glasses: Fulcher versus power law. Phys. Rev. B **185**, *32*, 516-519.

(50) Poddar, P.; Telem-Shafir, T.; Fried, T.; Markovich, G. Dipolar interactions in two- and three-dimensional magnetic nanoparticle arrays. *Phys. Rev. B* **2002**, *66*, 060403.

(51) Ying, Y.; Wang, L.; Li, W.; Qiao, L.; Zheng, J.; Yu, J.; Cai, W.; Jiang, L.; Che, S.; Zhang, L. Spin Glass in a Geometrically Frustrated Magnet of $ZnFe_2O_4$ Nanoparticles. *J. Supercond. Nov. Magn.* **2018**, *31*, 3553-3558.

(52) Gunnarsson, K.; Svedlindh, P.; Nordblad, P.; Lundgren, L.; Aruga, H.; Ito, A. Dynamics of an Ising Spin-Glass in the Vicinity of the Spin-Glass Temperature. *Phys. Rev. Lett.* **1988**, *61*, 754-757.

(53) Vijayanandhini, K.; Kutty, T. R. N. Magnetically tuneable nonlinear electronic properties of ZnO/La(Sr)MnO_3 ceramic composites. *J. Phys. D: Appl. Phys.* **2006**, *39*, 2902-2914.

(54) Andreanov, A.; Chalker, J. T.; Saunders, T. E.; Sherrington, D. Spin-glass transition in geometrically frustrated antiferromagnets with weak disorder. *Phys. Rev. B* **2010**, *81*, 014406.

(55) Lei, H.; Abeykoon, M.; Wang, K.; Bozin, E. S.; Ryu, H.; Graf, D.; Warren J. B.; Petrovic, C. Physical properties of $K_xNi_{2-x}Se_2$ single crystals. *J. Phys.: Conden. Matter* **2014**, *26*, 015701.

(56) Neilson, J. R.; Llobet, A.; Stier, A. V.; Wu, L.; Wen, J.; Tao, J.; Zhu, Y.; Tesanovic, Z. B.; Armitage N. P.; McQueen, T. M. Mixed-valence-driven heavy-fermion behavior and superconductivity in KNi_2Se_2. *Phys. Rev. B* **2012**, *86*, 054512.

(57) Fogle, W.; Ho, J. C.; Philipps, N. E. Concentration and temperature dependence of the magnetic heat capacity of dilute $CuMn_x$. *J. Phys. Colloques* **1978**, *39*, C6-901-C6-902.

(58) Harada, T.; Transport Properties of Iron Dichalcogenides FeX_2 (X = S, Se and Te).*J. Phys. Soc. Jpn.* **1998**, *67*, 1352-1358.

(59) Wang, K.; Wang, A.; Tomic, A.; Wang, L.; Abeykoon, A. M.; Dooryhee, E.; Billinge S. J.; Petrovic, C. Enhanced thermoelectric power and electronic correlations in $RuSe_2$. *Appl. Phys. Lett. Materials* **2015**, *3*, 041513.

(60) Matsuura, M.; Endoh, Y.; Hiraka, H.; Yamada, K.; Mischenko, A. S.; Nagaosa N.; Solovyev, I. V. Classical and quantum spin dynamics in the fcc antiferromagnet NiS_2 with frustration. *Phys. Rev. B* **2003**, *68*, 094409.

(61) Timirgazin, M. A.; Igoshev, P. A.; Arzhinikov A. K.; Irkhin, V. Yu. Magnetic states, correlation effects and metal-insulator transition in FCC lattice. *J. Phys. Condens. Matter* **2016**, *28*,505601.

(62) Kimber, A. J. S.; Chatterji, T. Spin-driven symmetry breaking in the frustrated fcc pyrite MnS_2. *J. Phys. Condens. Matter* **2015**, *27*, 226003.

(63) Diep, H. T.; Ghazali, A.; Berge B.; Lallemand, P. Phase Diagrams in f.c.c. Binary Alloys: Frustration Effects. *Europhys. Lett.* **1986**, *2*, 603-609.

(64) Jaglicic, Z.; Vrtnik, S.; Feuerbacher, M.; Dolinsek, J. Magnetic properties of $FeAl_2$ and and Fe_2Al_5. *Phys. Rev. B* **2011**, *83*, 224427.

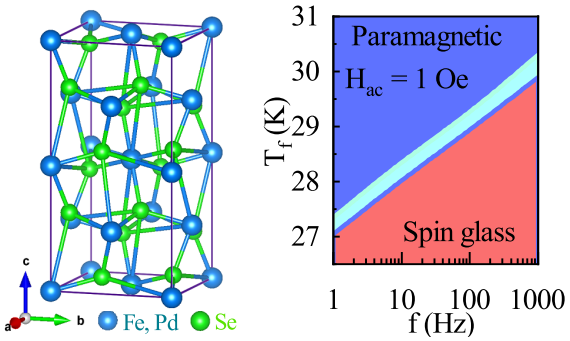

Figure 5: (TOC graphics and synopsis) Whereas pyrite structure is a high-temperature polymorph for both $FeSe_2$ and $PdSe_2$, here we report synthesis of pyrite $Fe_{0.36(4)}Pd_{0.64(4)}Se_2$ single crystals using ambient pressure chalcogenide flux. By combining experimental and theoretical methods, we show that $Fe_{0.36(4)}Pd_{0.64(4)}Se_2$ features magnetic spin glass state. The emergent property of polymorph alloy is different from those of the end members and it stems from random occupancies of metal atoms on the same atomic state.